Tensor-Based K-Nearest Neighbors Approach for Enhanced Neutron–Gamma Discrimination

Imane Ahnouz[1*], *Hanan* Arahmane[2*], and *Rajaa* Sebihi[1]

[1]LPHE-Modeling and Simulation, Faculty of sciences, Mohammed V University in Rabat, B.P. 1014 RP, Rabat, Morocco
[2]Paris-saclay University, CEA, List, F-91120 Palaiseau, France

Abstract. Neutron detection is essential in nuclear safety, medical diagnostics, and high-energy physics. However, reliably discriminating neutrons from gamma rays remains a major challenge in mixed radiation fields. This work investigates the performance of a K-Nearest Neighbors (KNN) classifier applied to features extracted through two Tucker decomposition–based signal separation methods: Multiway Blind Source Separation (MBSS) and Sequentially Truncated Multilinear Singular Value Decomposition (ST-MLSVD). The approach yielded high discrimination performance, with all tested configurations achieving a Figure of Merit (FOM) ranging from 1.61 to 3.91 and an F1 score of 100%. In particular, the MBSS–KNN and ST-MLSVD–KNN combinations in mode 2 produced the most reliable outcomes, combining robustness with strong accuracy for neutron–gamma classification. These results confirm the relevance of tensor-based feature extraction coupled with supervised learning, offering a promising pathway for reliable particle identification in complex radiation environments.

Keywords: Neutron-gamma discrimination, Scintillation detectors, Tucker decomposition, K-Nearest Neighbors (KNN).

1 Introduction

Neutron–gamma discrimination is a key challenge in radiation detection, with critical applications in nuclear nonproliferation monitoring, homeland security, neutron imaging, and high-energy physics. Scintillation detectors are widely employed for this task owing to their high efficiency, fast timing response, and real-time capability. However, in mixed radiation fields, pulses from neutrons and gamma rays often exhibit overlapping amplitudes and similar temporal characteristics, especially under high counting rates or low signal-to-noise conditions. These effects hinder accurate event separation and increase the risk of misclassification [1].

* Corresponding author: imane.ahnouz@gmail.com
hanan.arahmane@gmail.com

Classical pulse shape discrimination (PSD) methods, which exploit differences in scintillation decay times, have long been employed to distinguish neutrons from gamma rays. However, their performance decreases under low light conditions, high noise, or variable detector settings, and hardware-based implementations often lack flexibility across detectors and operational environments [2].

To overcome these limitations, machine learning (ML) techniques have been increasingly integrated into PSD frameworks. Supervised algorithms such as support vector machines (SVM) [3], k-nearest neighbors (KNN) [4], and artificial neural networks (ANN) [5], trained on labeled PSD features, have demonstrated superior performance by learning complex decision boundaries and improving both accuracy and robustness. In contrast, unsupervised approaches such as k-means clustering [6] and principal component analysis (PCA) [7] are mainly applied for feature extraction or exploratory analysis without labeled data, and generally achieve lower classification performance [8].

Beyond PSD-based approaches, blind source separation (BSS) methods have emerged as powerful tools for analyzing complex neutron–gamma datasets. Tensor decompositions such as canonical polyadic (CP) [9] and nonnegative tensor factorization (NTF) [10] exploit the multiway structure of radiation measurements to isolate latent sources and reduce dimensionality while preserving discriminative information. When combined with supervised classifiers, these decompositions can substantially improve class separability and robustness to noise and signal overlap [11].

Building on recent advances in Blind Source Separation (BSS), Tucker decomposition (TD) offers a flexible and computationally efficient framework for capturing higher-order correlations across modes. Its adaptability in rank selection enables richer feature representations, making it effective for analyzing multidimensional datasets. TD-based approaches, already applied in various domains [12,13], have demonstrated high accuracy in complex signal classification tasks [9]. In the context of radiation detection, however, this study introduces the first application of TD specifically to neutron–gamma discrimination. In particular, multilinear blind source separation (MBSS) and sequentially truncated multilinear singular value decomposition (ST-MLSVD) are Tucker-based methods that efficiently separate mixed radiation signals while preserving critical classification features, highlighting the potential of TD as a powerful tool for nuclear applications and radiation detection [14,15].

This study applies a KNN classifier to features extracted via MBSS and ST-MLSVD for neutron–gamma discrimination using scintillation detectors. Classification performance is quantified using the F1 score, which evaluates overall accuracy and balance between precision and recall. Separately, the Figure of Merit (FOM) is employed as a supervised validation metric within the KNN framework, assessing the quality of class separation based on the distribution of predicted labels relative to ground truth. To our knowledge, this is the first application of FOM in this form with KNN, representing a novel approach that highlights both classification accuracy and class separability. By combining TD-based feature extraction with these complementary metrics, this study offers new insights into neutron–gamma signal processing and demonstrates a significant advancement in nuclear radiation detection.

The paper describes the experimental setups and details the implementation of MBSS and ST-MLSVD in combination with KNN. A comparative analysis of their performance is presented, followed by a discussion of the main findings and potential directions for advancing tensor-based ML methods in radiation detection systems.

2 Materials and methods

https://doi.org/10.1051/e3sconf/202568000088

This section presents the experimental setup and the methodology employed for neutron–gamma discrimination in the current study.

2.1 Experimental setups

This study reports two experimental investigations of neutron–gamma radiation detection.

In the first experiment, approximately 30,000 signals were recorded using a plutonium–beryllium (PuBe) source producing a mixed neutron–gamma field, measured via the Time of Flight (TOF) method. Four YAP:Ce detectors were positioned ∼10 cm from the source with slight out-of-plane variations, recording low-energy cascade gamma rays from ^{234}U and 4.44 MeV gamma rays. The source and detectors were enclosed in a water-shielded cube with 500 mm thick walls. A NE-213A liquid scintillator, housed in a lead casing with a 10×10 mm aperture, was placed 925 mm from the source center, aligned along its cylindrical axis. Tagged neutron events were identified by the coincidence of 4.44 MeV gamma rays in the YAP:Ce detectors and fast neutrons in the NE-213A detector, along with prompt gamma-ray events detected by both detectors. Data acquisition was performed using a CAEN VX1751 Waveform Digitizer (10-bit resolution, 500 MHz bandwidth) [14,16]. The dataset is publicly accessible [17].

In the second experiment, 14,404 neutron–gamma pulses were acquired using an americium–beryllium ($^{241}\mathrm{Am}-\mathrm{Be}$) source with an average neutron energy of 4.5 MeV. Pulses were measured with an EJ299-33 plastic scintillator coupled to a TPS2000B digital oscilloscope. Signals were preamplified, amplified, and recorded by the oscilloscope operating at a 200 MHz bandwidth, 1 GS/s sampling rate, and 8-bit vertical resolution, with a 500 mV trigger threshold (∼1.6 MeV) [14]. This dataset is also publicly accessible [18].

2.2 Methodology processing

2.2.1 Tucker Decomposition

TD is a multilinear generalization of matrix factorization techniques, such as singular value decomposition (SVD), to higher-order tensors. It factorizes an N-th order tensor $\underline{\mathbf{Y}} \in \mathbb{R}^{I_1\times I_2\times\ldots\times I_n}$ into a low-dimensional core tensor tensor $\underline{\mathbf{G}} \in \mathbb{R}^{J_1\times J_2\times\ldots\times J_n}$ and a set of orthogonal factor matrices $\mathbf{U}^{(\boldsymbol{n})} \in \mathbb{R}^{I_n\times J_n}$ along each mode:

$$\underline{\mathbf{Y}} \approx \underline{\mathbf{G}} \times_1 \mathbf{U}^{(1)} \times_2 \mathbf{U}^{(2)} \times \ldots \times_N \mathbf{U}^{(N)} \tag{1}$$

The core tensor $\underline{\mathbf{G}}$ encodes the multilinear relationships between components, while the factor matrices define the principal subspace along each mode, capturing interactions across temporal, spectral/energy, and event/acquisition dimensions. TD enables efficient representation of multidimensional signals and extraction of meaningful latent features [9].

In this study, two TD-based methods—MBSS and ST-MLSVD—were applied to scintillation detector signals. A tensor $\underline{\mathbf{Y}} \in \mathbb{R}^{100\times 70\times 5}$ was constructed, with the third mode containing five representative signals [10,14]. The decomposition produced a core tensor $\underline{\mathbf{G}} \in \mathbb{R}^{5\times 5\times 5}$ and factor matrices $\mathbf{U}^{(1)} \in \mathbb{R}^{(100\times 5)}$, $\mathbf{U}^{(2)} \in \mathbb{R}^{(70\times 5)}$, and $\mathbf{U}^{(3)} \in \mathbb{R}^{(5\times 5)}$, capturing temporal, spectral, and event-based (acquisition) variations.

To enhance source separation, the Equivariant Robust Independent Component Analysis (ERICA) algorithm was incorporated as a penalized matrix factorization constraint, improving the separation of mixed radiation components. Both TD decomposition methods were implemented using the TDALAB toolbox [14,19], and the extracted features were subsequently employed for neutron–gamma classification using a KNN model.

2.2.2 Multiway Blind Source Separation

MBSS builds upon TD by incorporating additional constraints to mitigate the non-uniqueness problem inherent in classical TD. In standard TD, multiple sets of factor matrices can yield similar tensor approximations, leading to ambiguities when interpreting latent components. MBSS applies BSS principles to guide the factorization, ensuring that the extracted components are physically meaningful and stable, which is essential for applications like neutron–gamma discrimination.

Mathematically, the TD can be expressed using the Moore–Penrose pseudo-inverse:

$$\underline{\mathbf{Y}} = [\underline{\mathbf{G}} \times_1 \mathbf{Q}^{(1)^{\dagger}} \times_2 \mathbf{Q}^{(2)^{\dagger}} \ldots \times_N \mathbf{Q}^{(N)^{\dagger}}] \times_1 (\mathbf{U}^{(1)}\mathbf{Q}^{(1)}) \ldots \times_N (\mathbf{U}^{(N)}\mathbf{Q}^{(N)}) \tag{2}$$

where $\mathrm{Q}^{(n)}$is nonsingular and $\mathrm{Q}^{(n)^{\dagger}}$ denotes its pseudo-inverse.

The mode-n unfolding of $\underline{\mathbf{Y}}$ is approximated as:

$$\mathbf{Y}_{(n)} \approx \mathbf{U}^{(n)}\mathbf{B}^{(n)T}, \quad (n = 1,2,\ldots,N) \tag{3}$$

with $\mathbf{B}^{(n)} = \left[\mathbf{G}_{(n)}(\otimes_{p\neq n} \mathbf{U}^{(p)})^T\right]^T$ has a Kronecker structure, and $\mathbf{G}_{(n)}$ is the mode-n unfolding matrix of the core tensor $\underline{\mathbf{G}}$.

Factor matrices $\mathbf{U}^{(n)}$ are estimated via BSS algorithms, with the estimated matrix expressed as:

$$\widehat{\mathbf{A}}^{(n)} = \Psi_n\big(\mathbf{Y}_{(n)}\big) = \Psi_n\big(\mathbf{U}^{(n)}\mathbf{B}^{(n)T}\big) = \mathbf{U}^{(n)}\mathbf{P}_n\mathbf{D}_n \tag{4}$$

where $\Psi_n(.)$ represents the BSS procedure, and $\mathbf{P}_n$ and $\mathbf{D}_n$ account for permutation and scaling ambiguities. Mode-specific constraints, such as those imposed by ERICA, can incorporate prior physical knowledge, improving robustness to noise and signal transformations.

MBSS supports two extraction strategies:

1. Independent extraction: Each factor matrix $\mathbf{U}^{(n)}$ is estimated individually, followed by reconstruction of the core tensor:

$$\widehat{\underline{\mathbf{G}}} = \underline{\mathbf{Y}} \times_1 \mathbf{U}^{(1)^{\dagger}} \times_2 \mathbf{U}^{(2)^{\dagger}} \ldots \times_N \mathbf{U}^{(N)^{\dagger}} \tag{5}$$

When only the first $K < N$ factor matrices are reliably estimated, a partial TD is performed:

$$\underline{\mathbf{Y}} \approx \underline{\breve{\mathbf{G}}} \times_1 \mathbf{U}^{(1)} \times_2 \mathbf{U}^{(2)} \ldots .\times_K \mathbf{U}^{(K)} \tag{6}$$

with partial core tensor $\underline{\breve{\mathbf{G}}} \in \mathbb{R}^{J_1 \ldots \times J_K \times I_{K+1} \ldots \times I_N}$ computed as:

$$\underline{\breve{\mathbf{G}}} = \underline{\mathbf{G}} \times_{K+1} \mathbf{U}^{(K+1)} \times_{K+2} \mathbf{U}^{(K+2)} \ldots .\times_N \mathbf{U}^{(N)} \tag{7}$$

Finally, the estimated partial core tensor is obtained as:

$$\widehat{\underline{\breve{\mathbf{G}}}} = \underline{\mathbf{Y}} \times_1 \mathbf{U}^{(1)^{\dagger}} \times_2 \mathbf{U}^{(2)^{\dagger}} \ldots \times_K \mathbf{U}^{(K)^{\dagger}} \tag{8}$$

2. Sequential extraction: Factor matrices are determined one at a time, with the tensor updated at each iteration. This reduces dimensionality and computational cost, which is advantageous when the number of latent sources is smaller than the data dimensions.

Two main interpretations exist for constrained TD in MBSS:

- Physically interpretable sources: Each column of $\mathbf{U}^{(n)}$ corresponds to a latent source, and the core tensor $\underline{\mathbf{G}}$ encodes their interactions. In this interpretation, $\underline{\mathbf{Y}}$ represents a multidimensional mixture of independent sources.
- Transformed signal representation: The core tensor $\underline{\mathbf{G}}$ represents the true N-dimensional signal, while factor matrices act as transformation bases (e.g., time–frequency dictionaries), capturing filtering or distortion effects.

In this study, the first interpretation is adopted, aligning with the goal of neutron–gamma source separation and providing greater physical interpretability [14].

2.2.3 Sequentially Truncated Multilinear Singular Value Decomposition

ST-MLSVD extends classical MLSVD by applying sequential truncation of singular values along each mode, which enhances computational efficiency while providing a low-rank approximation of the original tensor. This method is particularly well-suited for high-dimensional datasets, such as multidimensional neutron–gamma signals.

Given an N-th order tensor $\underline{\mathbf{Y}} \in \mathbb{R}^{I_1 \times I_2 \times \ldots \times I_N}$, ST-MLSVD computes a low-rank approximation:

$$\underline{\mathbf{Y}} \approx \left(\widehat{\mathbf{U}}^{(1)}, \widehat{\mathbf{U}}^{(2)}, \ldots, \widehat{\mathbf{U}}^{(N)}\right) \times \underline{\widehat{\mathbf{G}}} \tag{9}$$

where $\widehat{\mathbf{U}}^{(k)} \in \mathbb{R}^{I_k \times R_k}$ are orthonormal factor matrices for mode k, $\underline{\widehat{\mathbf{G}}} \in \mathbb{R}^{R_1 \times R_2 \times \ldots \times R_N}$ is the truncated core tensor, R_N is the multilinear rank along mode-k, and p indicates the sequential processing order.

The algorithm proceeds by unfolding the tensor along each mode k into a matrix and performing a truncated SVD:

$$\mathbf{Y}_{(k)} = \mathbf{U}_k \mathbf{S}_k \mathbf{V}_k^T \tag{10}$$

where $\mathbf{U}_k$ contains the left singular vectors, $\mathbf{S}_k$ is a diagonal matrix of singular values, and $\mathbf{V}_k^T$ contains the right singular vectors.

Only the top R_k singular values and corresponding vectors are retained, effectively projecting the data onto a lower-dimensional subspace. Factor matrices are further processed with ERICA :

$$\widehat{\mathbf{U}}^{(k)} = \Psi_k\left(\mathbf{Y}_{(k)}\right) \tag{11}$$

2.2.4 Equivariant Robust Independent Component Analysis

ERICA serves as a penalized matrix factorization constraint, promoting statistical independence among components and aligning factor matrices with the physical characteristics of neutron–gamma signals. Its objective function is:

$$J(\mathbf{Y}) = \sum_{i=1}^{N} C_{(n_1, n_2, \ldots, n_q, Y_i)} \tag{12}$$

where $J(\mathbf{Y})$ is the objective function to be minimized, and $C_{(n_1, n_2, \ldots, n_q, Y_i)}$ represents the q-th order cumulant of the estimated sources.

Optimization uses a quasi-Newton method:

$$\theta_{k+1} = \theta_k - \alpha_k \boldsymbol{H}_k{}^{-1} \nabla J(\theta_k) \tag{13}$$

where $\alpha_k$is the learning rate, $\boldsymbol{H}_k$ is an approximation of the Hessian matrix, and $\nabla J(\theta_k)$ is the gradient at iteration k.

By maximizing statistical independence across all tensor modes, ERICA ensures robust separation of neutron–gamma signals, even in large or noisy datasets [14].

In this study, features extracted via TD-based methods (MBSS or ST-MLSVD) are subsequently classified using a KNN model, forming a two-stage pipeline that efficiently isolates mixed sources, preserves key discriminative information, and achieves highly accurate neutron–gamma discrimination. This integration of tensor decomposition with supervised learning represents a notable advancement in radiation signal analysis.

2.2.5 K-Nearest Neighbors

The KNN is a supervised classification method widely used in pattern recognition and signal discrimination, including neutron–gamma separation. Each detected pulse is represented by a feature vector extracted from the signal using TD-based methods (MBSS and ST-MLSVD), which decompose the data into three factor matrices. Two principal components (PCs) are selected from each factor matrix based on their correlation ρ with pure neutron and gamma events [14], forming mode-specific feature vectors:

$$\mathbf{X}_i^{(k)} = \begin{bmatrix} C_{i,1}^{(k)} \\ C_{i,2}^{(k)} \end{bmatrix}, k = 1,2,3 \tag{14}$$

where $C_{i,j}^{(k)}$ represents the j-th component of the i-th sample in mode k, and each vector is labeled as 0 (gamma) or 1 (neutron).

The dataset is divided into training and test subsets. For a test sample, KNN identifies its K nearest neighbors in the feature space and assigns the class corresponding to the majority vote. The similarity between feature vectors is quantified using the Euclidean distance:

$$d_i^{(k)} = \sqrt{\left(C_{i,1,test}^{(k)} - C_{i,1,train}^{(k)}\right)^2 + \left(C_{i,2,test}^{(k)} - C_{i,2,train}^{(k)}\right)^2} \tag{15}$$

where $C_{1,test}^{(k)}$ and $C_{2,test}^{(k)}$ are the two PCs of the test sample, and $C_{i,1}^{(k)}$ and $C_{i,2}^{(k)}$ are those of the i-th training sample.

In this study, the number of neighbors K was selected empirically to balance bias and variance. A uniform weighting scheme was applied, meaning that each neighbor contributed equally to the classification decision. These parameter choices ensure a fair comparison across modes and reduce the risk of overfitting given the limited dataset.

The KNN classifier is applied independently to the feature vectors of each mode, allowing evaluation of the discriminatory power of mode-specific components. The detailed application procedure is described in Section 3.1.

2.3 Performance metrics

2.3.1 Figure of Merit

The FOM quantifies the effectiveness of neutron–gamma discrimination by measuring the separation between the two signal distributions. It is defined as :

$$FOM = \frac{S}{\mathrm{FWHM_n} + \mathrm{FWHM_\gamma}} \tag{16}$$

where S is the distance between the centroids of the neutron and gamma-ray distributions, and $\mathrm{FWHM_n}$ and $\mathrm{FWHM_\gamma}$ correspond to the full widths at half maximum of the neutron and gamma peaks, respectively. A higher FOM (typically ≥ 1.27) indicates more effective discrimination between the two particle types [1].

2.3.2 F1 score

The F1 score is a key metric for evaluating the performance of neutron–gamma discrimination algorithms, providing a balanced measure by combining precision (P_r) and recall (R_e):

$$\text{F1 score} = 2 \times \frac{P_r \times R_e}{P_r + R_e} \tag{17}$$

Precision quantifies the fraction of correctly identified gamma events among all events predicted as gamma:

$$P_r = \frac{TP}{TP + FP} \tag{18}$$

where TP denotes true gamma events correctly classified, and FP corresponds to neutron events incorrectly labeled as gamma.

Recall (R_e) measures the proportion of actual gamma events correctly detected:

$$R_e = \frac{TP}{TP + FN} \tag{19}$$

with FN representing gamma events misclassified as neutrons.

By integrating both precision and recall, the F1 score accounts simultaneously for false positives and false negatives, offering a robust and informative metric for assessing overall discrimination performance [20].

3 Results and discussion

This section evaluates the performance of the KNN classifier combined with TD methods, using two complementary metrics: the traditional FOM, which quantifies the degree of separation between neutron and gamma classes, and the F1 score, which reflects overall classification accuracy by jointly accounting for precision and recall. To complement the quantitative analysis, visualizations of decision boundaries are provided for each decomposition mode (temporal, spectral, acquisition) and for both experimental setups using different scintillation detectors.

3.1 Application of KNN

The initial 2D pulse signals were reorganized into a third-order tensor to enable Tucker decomposition. This tensor was decomposed using both MBSS and ST-MLSVD methods, producing three mode-specific factor matrices representing the temporal, spectral, and acquisition dimensions. For each mode, two PCs were selected from the corresponding factor matrix based on their correlation with pure neutron and gamma reference signals, forming discriminative feature vectors as introduced in our previous work [14]. The resulting features were normalized using z-score scaling and labeled according to their known pulse origin (1 for neutron, 0 for gamma). The dataset was then divided into 70 % training and 30 % test samples. To ensure optimal classification, the number of neighbors K was empirically varied from 1 to 20, using the Euclidean distance and a uniform weighting scheme. The configuration achieving the highest F1-score was retained. This supervised approach enables a consistent and rigorous evaluation of the discriminative capability of each mode.

3.2 Neutron–Gamma Discrimination Results from the PuBe Source Experiment

As mentioned above, the KNN classifier was applied independently to each mode using the Euclidean distance and a uniform weighting scheme. The number of neighbors K was empirically selected within the range $1 \leq \mathrm{K} \leq 20$ for each mode based on the characteristics of the mode-specific feature vectors. For the temporal mode (mode 1), which is more susceptible to noise, a larger neighborhood size ($K = 15$) was chosen to stabilize the classification. The spectral mode (mode 2), being highly discriminative, required only a small K ($K = 2$) to preserve the fine separation between neutron and gamma signals. For the event mode (mode 3), an intermediate value ($K = 5$) provided a balanced trade-off between robustness and sensitivity. These selections reflect the interplay between feature dimensionality, discriminative power, and noise, ensuring optimal classification performance across all modes.

3.2.1 FOM results

Classical FOM, commonly used in PSD, assumes one-dimensional Gaussian-like distributions, which limits its applicability in multi-dimensional ML-based approaches. In this work, we applied a generalized FOM directly to the distributions of continuous decision scores obtained from KNN classification along each tensor mode $\mathbf{U}^{(n)}$ (temporal, spectral, event) extracted via MBSS and ST-MLSVD. The FOM is explicitly defined as:

$$FOM = \frac{S}{\mathrm{FWHM_n} + \mathrm{FWHM}_\gamma} = \frac{|\mu_n - \mu_\gamma|}{2.355 \times (\sigma_n + \sigma_\gamma)} \tag{20}$$

where μ_n, and μ_γ are the mean values of the decision scores assigned to the neutron and gamma classes, respectively, and σ_n and σ_γ are their standard deviations. The factor 2.355 converts the standard deviation to the FWHM assuming Gaussian-like distributions.

It should be emphasized that the decision scores correspond to the continuous probabilities/scores returned by KNN, reflecting the fraction of neighbors belonging to each class, rather than the discrete class labels (0 or 1). This ensures that the calculation of σ is meaningful. Such a mode-wise evaluation enables independent quantification of class separability across temporal, spectral, and event features, providing a more rigorous and accurate assessment than the classical one-dimensional FOM.

Table 1. FOM values for MBSS–KNN and ST-MLSVD–KNN across each mode.

Method	Mode 1	Mode 2	Mode 3
MBSS–KNN	2.45	3.91	1.61
ST-MLSVD–KNN	2.45	3.91	1.72

As shown in Table 1, both MBSS–KNN and ST-MLSVD–KNN achieved high and nearly identical FOM values in mode 1 (temporal) and mode 2 (spectral), reflecting effective capture of dominant signal features such as pulse shape, decay characteristics, and energy distribution. These results surpass those reported by Mauritzson et al. [21], who employed a TOF-based neutron tagging technique and obtained intrinsic FOM values of up to approximately 1.6. In mode 3 (event), ST-MLSVD–KNN outperforms MBSS–KNN (1.72 vs. 1.61), due to its ability to exploit higher-order inter-modal correlations and suppress noise via sequential singular value truncation. This is particularly important for the NE-213A detector, where variations in event characteristics generate complex mixtures of neutron and gamma pulses. MBSS, assuming statistical independence, is less effective, whereas ST-MLSVD preserves critical event-related correlations across tensor modes, enhancing feature discriminability.

These results demonstrate that TD-based signal separation combined with KNN, together with the generalized FOM metric, ensures robust and accurate classification across temporal, spectral, and event modes, outperforming the K-means model reported in [14].

3.2.2 F1 score results

The classification performance of MBSS and ST-MLSVD, based on TD across temporal, spectral, and event modes, was evaluated using Precision, Recall, and F1 score via a KNN classifier.

Table 2. Classification performance of MBSS–KNN and ST-MLSVD–KNN across all modes.

Mode	Method	Precision	Recall	F1 score
Mode 1	MBSS–KNN	1	1	1
	ST-MLSVD–KNN	1	1	1
Mode 2	MBSS–KNN	1	1	1
	ST-MLSVD–KNN	1	1	1
Mode 3	MBSS–KNN	1	0.90	0.95
	ST-MLSVD–KNN	1	1	1

As shown in Table 2, both MBSS–KNN and ST-MLSVD–KNN achieved perfect classification in modes 1 and 2, demonstrating flawless identification of neutron and gamma pulses with no false positives or missed events. In mode 3, ST-MLSVD–KNN maintained perfect performance across all metrics, whereas MBSS–KNN achieved a precision of 100% but a recall of 90%, indicating that while all neutron events were correctly classified (no false positives), 10% of gamma events were misclassified as neutrons (false negatives). This partial misclassification reduced the overall F1 score to 95%, reflecting that MBSS–KNN remains highly effective in the event mode but is slightly less capable than ST-MLSVD–KNN at capturing the complex event-related correlations inherent in gamma pulses. The lower recall highlights the challenge for MBSS in separating overlapping event features, which can arise from detector-induced mixing and noise, emphasizing the advantage of methods like ST-MLSVD that exploit higher-order inter-modal correlations.

These results indicate that ST-MLSVD–KNN consistently preserves discriminative features across all tensor modes, while MBSS–KNN performs slightly less effectively in the event mode, likely due to its limited ability to capture higher-order correlations. Overall, both TD-based methods combined with KNN provide robust neutron–gamma discrimination, with ST-MLSVD showing a slight advantage for complex multi-dimensional event features.

3.2.3 Visualization of Neutron–Gamma Class Separation

Visualization of class separation provides intuitive support for evaluating classification performance. In this study, two components extracted via TD were used, capturing the essential structure of the data across temporal, spectral, and event modes while preserving the most discriminative information. Representing the data in this two-dimensional feature space allows a visual assessment of neutron–gamma separation.

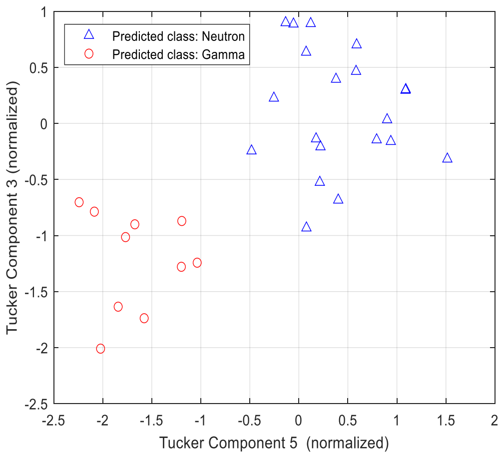

Fig. 1. Visualization of neutron–gamma separation in mode 1 using MBSS–KNN and ST-MLSVD–KNN.

Figure 1 shows clear separation between neutron and gamma events. The components extracted from mode 1 highlight distinct clustering in the feature space for both MBSS–KNN and ST-MLSVD–KNN, reflecting KNN’s ability to exploit temporal signatures to construct an effective decision boundary. This confirms that temporal features alone provide accuarte discrimination.

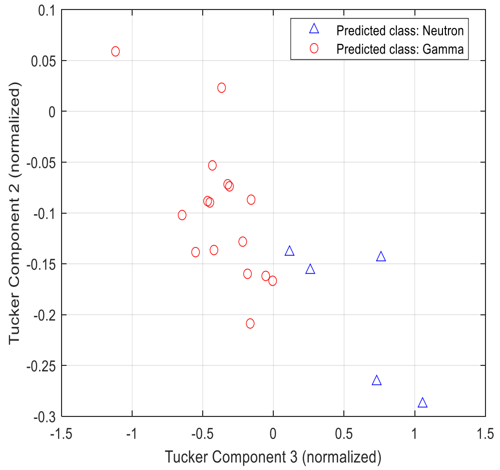

Fig. 2. Visualization of neutron–gamma separation in mode 2 using MBSS–KNN and ST-MLSVD–KNN.

Figure 2 illustrates two compact and well-separated clusters in the spectral domain. Mode 2 components capture energy-dependent differences between neutron and gamma events, enabling KNN to form a clear decision boundary. This demonstrates the discriminative power of spectral features for reliable neutron–gamma classification.

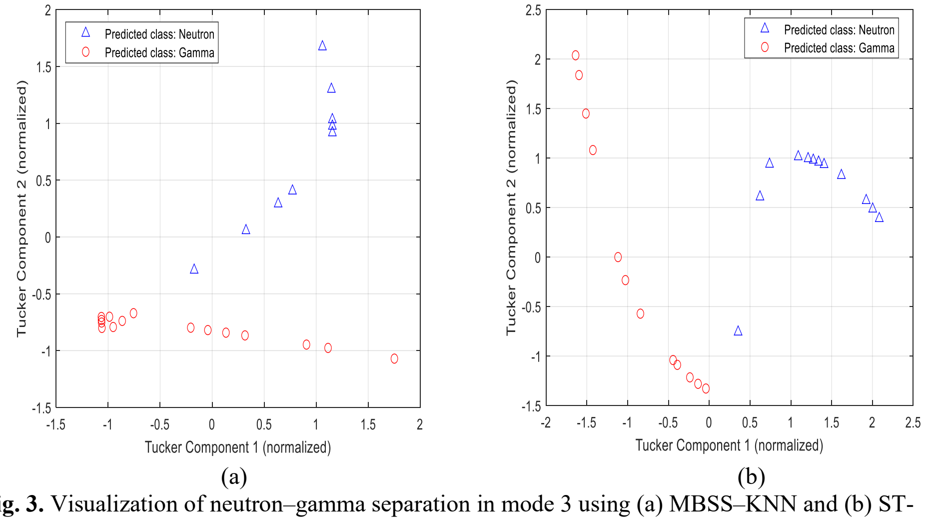

Fig. 3. Visualization of neutron–gamma separation in mode 3 using (a) MBSS–KNN and (b) ST-MLSVD–KNN.

Figure 3 illustrates the event mode separation for the two methods. With MBSS–KNN (Fig. 3a), the classes show partial clustering, with considerable overlap in the central feature-space region, limiting KNN's ability to define a reliable boundary. In contrast, ST-MLSVD–KNN (Fig. 3b) produces two compact, well-separated clusters, providing more homogeneous local neighborhoods. This highlights the effectiveness of ST-MLSVD in capturing event-specific correlations, enhancing classification performance in the event mode.

 https://doi.org/10.1051/e3sconf/202568000088

3.3 Neutron–Gamma Discrimination Results from the $^{241}\mathbf{Am}-\mathbf{Be}$ Source Experiment

In the second experiment, the KNN neighborhood size K was specifically chosen for each mode to optimize classification performance based on the characteristics of the extracted feature vectors: $K = 18$ for the temporal mode (mode 1), $K = 4$ for the spectral mode (mode 2), and $K = 5$ for the event mode (mode 3). These values reflect an empirical adjustment to balance stability, sensitivity, and discriminative resolution in each mode.

3.3.1 FOM results

The FOM results from the second experimental study are summarized in Table 3, comparing MBSS–KNN and ST-MLSVD–KNN across the three tensor modes.

Table 3. FOM values for MBSS–KNN and ST-MLSVD–KNN.

Method	Mode 1	Mode 2	Mode 3
MBSS–KNN	2.08	3.18	2.32
ST-MLSVD–KNN	2.08	3.18	2.26

As shown in Table 3, both methods consistently yield FOM values above 1.27 in all modes, demonstrating the robustness of the proposed approach for neutron–gamma discrimination. This performance surpasses that of the K-means method reported in [14] and the classical PSD technique, such as the Charge Comparison Method (CCM), which achieved a FOM of 1.04 [22]. The identical FOMs in modes 1 and 2 indicate that MBSS and ST-MLSVD are equally effective in capturing temporal and spectral features.

A notable difference occurs in mode 3, where MBSS–KNN achieves a higher FOM (2.32) than ST-MLSVD–KNN (2.26). This can be explained by the characteristics of the EJ299-33 plastic scintillator, which produces pulses with well-localized event signatures and minimal overlap between consecutive events. MBSS, which assumes signal independence and non-negativity, is therefore more effective at isolating individual event contributions, enhancing neutron–gamma discrimination. In contrast, ST-MLSVD leverages strong inter-modal correlations, which are less pronounced in the event mode, resulting in slightly lower FOM values.

These results highlight MBSS's advantage in handling event-mode data, where signals correspond to localized detector events, and demonstrate its potential for applications requiring precise exploitation of individual event responses.

3.3.2 F1 score results

The F1 score results from the second experimental study are summarized in Table 4, comparing MBSS–KNN and ST-MLSVD–KNN across the three tensor modes.

Table 4. Classification performance of MBSS–KNN and ST-MLSVD–KNN.

Mode	Method	Precision	Recall	F1 score
Mode 1	MBSS–KNN	1	1	1
	ST-MLSVD–KNN	1	1	1

Mode 2	MBSS–KNN	1	1	1
	ST-MLSVD–KNN	1	1	1
Mode 3	MBSS–KNN	1	1	1
	ST-MLSVD–KNN	0.92	1	0.96

As shown in Table 4, both methods achieved perfect scores in modes 1 and 2, indicating flawless classification of neutron and gamma pulses. In mode 3, MBSS–KNN maintained perfect precision, recall, and F1 score, while ST-MLSVD–KNN achieved slightly lower precision (92%) with recall at 100%, resulting in an F1 score of 96%. This indicates that all gamma events were correctly detected, while a small fraction of neutron events were misclassified.

Overall, the consistently high F1 scores across all modes confirm the strong discriminative capability and robustness of both TD-based methods for neutron–gamma separation, with MBSS showing a slight advantage in the event mode.

3.3.3 Visualization of Neutron–Gamma Class Separation

The visualization in the second experiment was performed using the same approach as in the first experiment, with two TD-extracted components forming a 2D feature space to assess neutron–gamma separation by MBSS–KNN and ST-MLSVD–KNN.

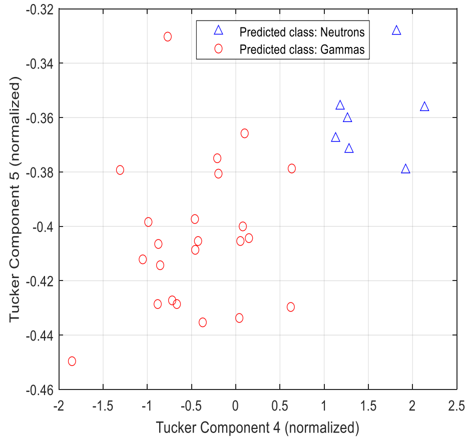

Fig. 4. Visualization of neutron–gamma separation in mode 1 (temporal) using MBSS–KNN and ST-MLSVD–KNN.

Figure 4 shows clear separation between neutron and gamma events. Both methods produce non-overlapping clusters, indicating that the temporal components from mode 1 effectively capture class-specific characteristics. This demonstrates the KNN classifier's ability to exploit temporal features to construct a reliable decision boundary.

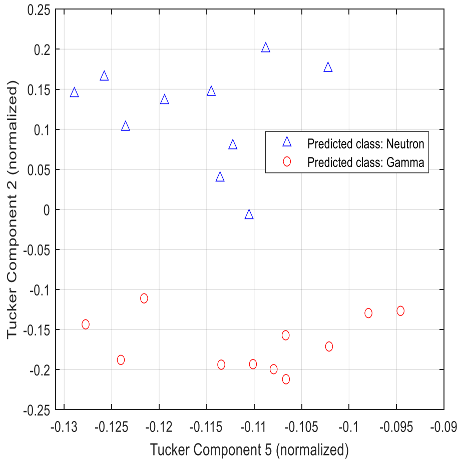

Fig. 5. Visualization of neutron–gamma separation in mode 2 (spectral) using MBSS–KNN and ST-MLSVD–KNN.

Figure 5 illustrates distinct clustering of neutron and gamma events along the spectral dimensions, with neutrons concentrated in the upper region and gammas in the lower region. The clear separation highlights the discriminative power of spectral features and confirms that KNN can leverage this information for accurate neutron–gamma discrimination.

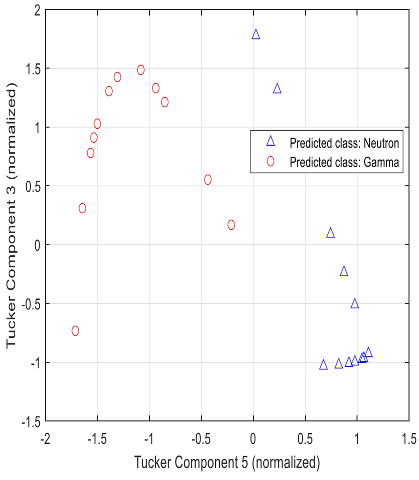

(a)

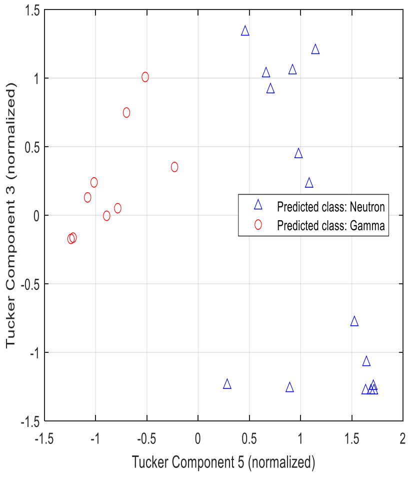

(b)

Fig. 6. Visualization of neutron–gamma separation in mode 3 (event) using (a) MBSS–KNN and (b) ST-MLSVD–KNN.

Figure 6 compares event mode separation for the two methods. With MBSS–KNN (Fig. 6a), neutron and gamma events form two compact, well-separated clusters along Component 5, providing a homogeneous feature space that enhances KNN's discriminative power. In contrast, ST-MLSVD–KNN (Fig. 6b) shows more dispersed events with partial overlap, particularly near the center, reducing local neighborhood homogeneity and limiting classification performance. Overall, these results indicate that MBSS–KNN offers robustness in the event mode, providing a more reliable and discriminative representation for neutron–gamma separation.

3.4 Comparative analysis: MBSS–KNN vs ST-MLSVD–KNN

Performance evaluation using FOM and F1 scores across both experiments shows that MBSS–KNN and ST-MLSVD–KNN achieve strong neutron–gamma discrimination. In temporal and spectral modes, both methods yield similar results, as dominant signal features—pulse shape, decay characteristics, and energy distribution—are effectively captured, allowing extraction of comparable and informative representations.

Differences appear in the event mode due to detector-specific characteristics. In the first experiment, ST-MLSVD–KNN outperforms MBSS–KNN by exploiting higher-order inter-modal correlations and mitigating noise, thereby preserving essential event-related patterns in complex, scattered signals. In contrast, during the second experiment, MBSS–KNN achieves better performance, as the detector generates well-localized events with minimal signal spread, aligning with MBSS assumptions of source independence and enhancing neutron–gamma separation accuracy.

Overall, both TD-based methods provide robust and reliable neutron–gamma discrimination across all modes and experimental conditions, with event-mode performance reflecting the interplay between detector properties and the assumptions inherent to each decomposition approach.

4 Conclusion

This study evaluated the performance of a KNN classifier applied to features extracted via two TD-based methods—MBSS and ST-MLSVD—for neutron–gamma discrimination using scintillation detectors. Two experiments were conducted to assess the robustness of the approach.

Results show that both methods achieve high and comparable performance in temporal (mode 1) and spectral (mode 2) modes. FOM values reached 2.45 and 3.91 in the first experiment, and 2.08 and 3.18 in the second, while F1 scores were 100% across both experiments and modes, confirming near-perfect separation. The KNN classifier effectively exploits these extracted features due to its non-parametric nature, establishing precise decision boundaries without assuming prior data distributions.

In the event mode (mode 3), performance differences emerge. In the first experiment, ST-MLSVD–KNN slightly outperformed MBSS–KNN, while in the second experiment, MBSS–KNN achieved better results. These variations reflect the influence of detector characteristics on event-mode discrimination, highlighting the importance of method–detector compatibility. Visualization of class separation further confirms consistent clustering and effective separation across all modes.

Overall, the TD-based KNN framework demonstrates robustness, reliability, and strong discriminative capability, making it suitable for practical applications in nuclear security, radiation monitoring, and neutron imaging. Its efficiency and accuracy render it promising for real-time and embedded systems. Future work will explore advanced detector configurations and the integration of TD with sophisticated ML and deep learning techniques, such as Convolutional Neural Networks (CNNs), to further enhance classification accuracy and generalization under complex detection conditions.

References

1. J. Boo and M. Jeong. Comparative Study of the Pulse Shape Discrimination (PSD) Performance of Pixelated Stilbene and Plastic Scintillator (EJ-276) Arrays for a Coded-

Aperture-Based Hand-Held Dual-Particle Imager. Nucl. Eng. Technol., **55**, 1677 (2023)

2. M. Sénoville, F. Delaunay, M. Pârlog, N.L. Achouri, N.A. Orr, Neutron-γ discrimination with organic scintillators: Intrinsic pulse shape and light yield contributions. Nucl. Instrum. Methods Phys. Res., Sect. A, **971**, 164080 (2020)
3. W. Zhang, T. Wu, B. Zheng, S. Li, Y. Zhang, Z.Yin, A Real-Time Neutron-Gamma Discriminator Based on the Support Vector Machine Method for the Time-of-Flight Neutron Spectrometer. Plasma Sci. Technol., **20**, 045601 (2018)
4. M. Durbin, M.A. Wonders, M. Flaska, A. T. Lintereur, K-Nearest Neighbors Regression for the Discrimination of Gamma Rays and Neutrons in Organic Scintillators. Nucl. Instrum. Methods Phys. Res., Sect. A, **987**, 164826 (2021)
5. N. M. Michels, A. J. Jinia, S. D. Clarke, H. -S. Kim, S. A. Pozzi and D. D. Wentzloff, Real-Time Classification of Radiation Pulses with Piled-Up Recovery Using an FPGA-Based Artificial Neural Network. IEEE Access, **11**, 78074-78083 (2023)
6. A. Hachem, Y. Moline, G. Corre, B. Ouni, M. Trocme, A. Elayeb, F. Carrel, Labeling Strategy to Improve Neutron/Gamma Discrimination with Organic Scintillator. Nucl. Eng. Technol., **55**, 4057 (2023)
7. T. Alharbi, Principal Component Analysis for Pulse-Shape Discrimination of Scintillation Radiation Detectors. Nucl. Instrum. Methods Phys. Res., Sect. A, **806**, 240 (2016)
8. T. Ma, H. Song, B. LYU and J. Ma, *Comparison of Artificial Intelligence Algorithms and Traditional Algorithms in Detector Neutron/Gamma Discrimination*, in Proceedings of the International Conference on Artificial Intelligence and Computer Engineering, ICAICE, pp. 173, 23-25 October 2020, Beijing, China (2020)
9. S. Rabanser, O. Shchur, S. Günnemann, Introduction to Tensor Decompositions and their Applications in Machine Learning. arXiv (2017)
10. H. Arahmane, E.-M. Hamzaoui, R.C. El Moursli, Improving Neutron-Gamma Discrimination with Stilbene Organic Scintillation Detector Using Blind Nonnegative Matrix and Tensor Factorization Methods. J. Spectrosc., **3**, 1–9 (2019)
11. H. Arahmane, E.-M. Hamzaoui, Y. Ben Maissa, R. Cherkaoui El Moursli, Neutron-Gamma Discrimination Method Based on Blind Source Separation and Machine Learning. Nucl. Sci. Tech., **32**, 18 (2021)
12. X. Li, D. Xu, H. Zhou, L. Li, Tucker Tensor Regression and Neuroimaging Analysis. Stat Biosci., **10**, 520–545 (2018)
13. G. Zhou, A. Cichocki, Fast and Unique Tucker Decompositions via Multiway Blind Source Separation. Bull. Pol. Acad. Sci. Tech. Sci., **60**, 389–405 (2012)
14. I. Ahnouz, H. Arahmane, R. Sebihi, Optimizing Neutron-Gamma Discrimination in Scintillation Detectors using Tucker Decomposition. Kuwait J. Sci., **53**, 100511 (2026)
15. A.A. Suárez-León, C. Varon, G. Goovaerts, C.R. Vázquez-Seisdedos, S. Van Huffel, *Irregular heartbeat detection using sequentially truncated multilinear singular value decomposition*, in: 2017 Computing in Cardiology, CinC, pp. 1–4, 24-27 September 2017, Rennes, France (2017)
16. H. Liu, P. Li, M. Liu, K. Wang, Z. Zuo, B. Liu, Pulse shape discrimination based on the Tempotron: a powerful classifier on GPU, IEEE Trans. Nucl. Sci., **71**, 2297-2308 (2024)
17. H. Liu, HaoranLiu507/TempotronGPU (2024). https://github.com/HaoranLiu507/TempotronGPU

18. R. Liu, P. Li, H. Liu, Dataset for neutron and gamma-ray pulse shape discrimination: radiation pulse signals and discrimination methodologies. Zenodo (2023). https://doi.org/10.5281/zenodo.7754573
19. G. Zhou and A. Cichocki, TDALAB: Tensor Decomposition Laboratory, LABSP, Wako-shi, Japan (Version 1.1), 2013. http://bsp.brain.riken.jp/TDALAB/
20. L. Liu and H. Shao, Study on Neutron–Gamma Discrimination Method Based on the KPCA-GMM-ANN. Radiat. Phys. Chem., **203**, 110602 (2023)
21. N. Mauritzson, K.G. Fissum, J.R.M. Annand, H. Perrey, R.J.W. Frost, R.A. Jebali, A. Backis, R. Hall-Wilton, K. Kanaki, V. Maulerova-Subert, C. Maurer, F. Messi, E. Rofors, Technique for the measurement of intrinsic pulse-shape discrimination for organic scintillators using tagged neutrons. Nucl. Instrum. Methods Phys. Res., Sect. A, **1039**, 167141 (2022)
22. S. Baselga and E. Montbarbon, Neutron and Gamma Pulse Shape Discrimination by Robust Determination of the Decay Shape. Applied Sciences, **14**, 5532 (2024)